Available online at www.sciencedirect.com
ScienceDirect
Journal of Solid State Chemistry 181 (2008) 693–699
JOURNAL OF SOLID STATE CHEMISTRY
www.elsevier.com/locate/jssc

Diffusion and phase transformations in spark plasma synthesized and sintered Cu–V_2O_5 couples

Jean-Philippe Monchoux*, Jean Galy

Centre d'Elaboration de Matériaux et d'Etudes Structurales—CNRS UPR 8011, 29, rue Jeanne Marvig, BP 94347, 31055 Toulouse Cedex 4, France

Received 15 July 2007; received in revised form 20 December 2007; accepted 30 December 2007
Available online 12 January 2008

Abstract

Fast diffusion of Cu into V_2O_5 at 520 °C is studied in Cu–V_2O_5 diffusion couples sintered by spark plasma sintering. The impact, on the diffusion profiles, of phase transformations and of variations of the diffusion coefficient with Cu concentration is discussed. From the pure Cu source, two phases are observed to spread, leading to a "two-step-like" shape of the diffusion profiles. In the more concentrated phase (phase ε), the diffusion coefficient D of Cu is $\approx 3\times10^{-8}$ m^2/s. This is a remarkably high value, of the same order of magnitude as self-diffusion in liquid metals. In the less concentrated phase (phase β'), D is lower than in ε. This is due to the differences in the diffusion mechanisms of Cu in these two phases: two dimensional in ε and one dimensional in β'. In β', D strongly depends on Cu concentration. This is in good agreement with computer simulations reported in the literature.

Keywords: Vanadium oxide bronzes; Diffusion; Phase transformations; Spark plasma sintering

1. Introduction

New insights into copper–vanadium oxide bronzes have been gained with the remarkable reversible copper extrusion–insertion into the layers of the $Cu_{2.33}V_4O_{11}$ bronze structure. This is likely to lead to a new type of electrode for rechargeable Li batteries [1]. Electrochemical tests on the $Cu_{2.33}V_4O_{11}$/Li system showed that Li displaces Cu during discharge thereby forming metallic Cu dendrites on the surface of the material grains. During recharge, Cu is reinserted in the structure between the $[V_4O_{11}]_n$ layers, while Li is removed from it, and the initial crystal structure is re-crystallized. Mass transport and phase transformations in vanadium oxides bronzes are then important issues from both fundamental and practical viewpoints.

Our aim here is to study the diffusion and phase transformations phenomena that occur in the Cu–V_2O_5 system. This system has been chosen because of its simplicity. Casalot et al. [2] showed that at 600 °C this system exhibits three $Cu_xV_2O_5$ phases, α, β' and ε with homogeneity ranges of $0<x<0.02$, $0.26<x<0.64$ and $0.85<x\leqslant1$, respectively. To get bulk samples from initial Cu and V_2O_5 powders, compaction by powder metallurgy techniques is required. As the β' and ε phases are tunnel and layer structured solids, respectively [3], diffusion and kinetics of phase transformations in this system are expected to be fast [4]. Then, compaction of the powders has to proceed very quickly to obtain bulk samples before significant reaction has taken place. Spark plasma sintering (SPS) has been proven to meet spectacularly the requirement of fast sintering of various materials [5]. The sintering mechanisms, not yet fully understood, involve the influence of electric current on mass transport [5] and on phase transformations [6], as well of the plastic deformation of the powder particles [7]. Here, we take advantage of the rapidity of synthesis by SPS to study the fast phenomena that occur during synthesis of the $Cu_xV_2O_5$ phases. Additionally, the method to probe mass transport developed here could be extended to other fast-ion conductors, for which diffusion coefficient measurements are known to be difficult [4]. Besides these fundamental questions, the SPS also opens a novel approach to synthesize these compounds.

*Corresponding author. Fax: +33 5 62 25 79 99.
E-mail address: monchoux@cemes.fr (J.-P. Monchoux).

0022-4596/$ - see front matter © 2008 Elsevier Inc. All rights reserved.
doi:10.1016/j.jssc.2007.12.040

2. Experimental

Powders of Cu (99.5% pure, particle size of about 400 μm) and V_2O_5 (99.6% pure) were used. Cu was first placed in a carbon die 8 mm in diameter and then V_2O_5 was added. Suitable amounts of powder were employed to yield, after compaction, layers of Cu and V_2O_5, 2 and 6 mm thick, respectively. Care was taken to avoid mixing between powders and to preserve planar interfaces between Cu and V_2O_5. The die was then placed on a Syntex 2080 SPS machine. Heating rate was ≈100 °C/min. A 75 MPa pressure was obtained in 2 min and the pulse sequence was set to 12:2 (i.e. twelve 3.2 ms periods "on" followed by two 3.2 ms periods "off"). When the desired temperature was reached (i.e. 520 °C), it was maintained through the duration of the experiment (between 2 and 32 min). Then, heating was stopped and the die was quenched in an Ar atmosphere, resulting in an initial ≈100 °C/min quenching rate. The resulting compaction was better than 95% of the theoretical density. Temperature was controlled with a thermocouple positioned at the periphery of the die. Under isothermal conditions, the accuracy of temperature measurements is ±3 °C.

The samples were then cut perpendicularly to their diameter and metallographically prepared (grinding by SiC papers and polishing by diamond pastes down to 3 μm). Growth of $Cu_xV_2O_5$ phase was followed by back-scattered electron (BSE) imaging and energy dispersive spectrometry (EDS) line-scans in a Jeol JSM 6700 F scanning electron microscope (SEM). EDS line-scan intensity of Cu I_{Cu} has been divided by the intensity I^0_{Cu} of pure Cu available on the same sample to obtain normalized values, irrespective of beam current fluctuations. These normalized values have been calibrated using $Cu_xV_2O_5$ standards of known Cu concentration (see Fig. 1). They have been prepared as follows: suitable amounts of Cu and V_2O_5 powders have been mixed and annealed in evacuated sealed quartz tubes at 600 °C for 24 h to achieve homogeneous single-phased $Cu_xV_2O_5$ samples. Then, the powders obtained were controlled by X-ray analyses to check that only the targeted phase remained in the samples. Finally, the powders were compacted by SPS to produce suitable bulk specimens for EDS analyses. Furthermore, given the large width of the analyzed area (some millimeters), the EDS signal intensity originating from a homogeneous material is

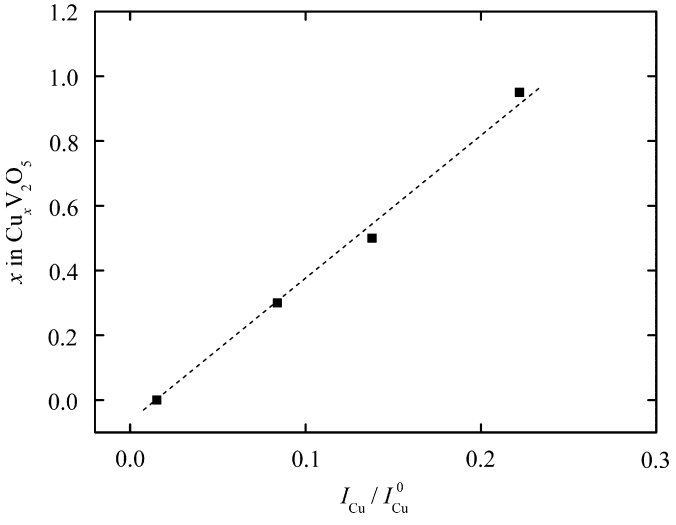

Fig. 1. Calibration curve of normalized EDS intensity. Cu concentration (expressed by x in $Cu_xV_2O_5$) of samples of known composition has been plotted as a function of the I_{Cu}/I^0_{Cu} ratio (with I_{Cu} and I^0_{Cu} standing for the intensity of EDS Cu signal from the sample and from pure Cu, respectively).

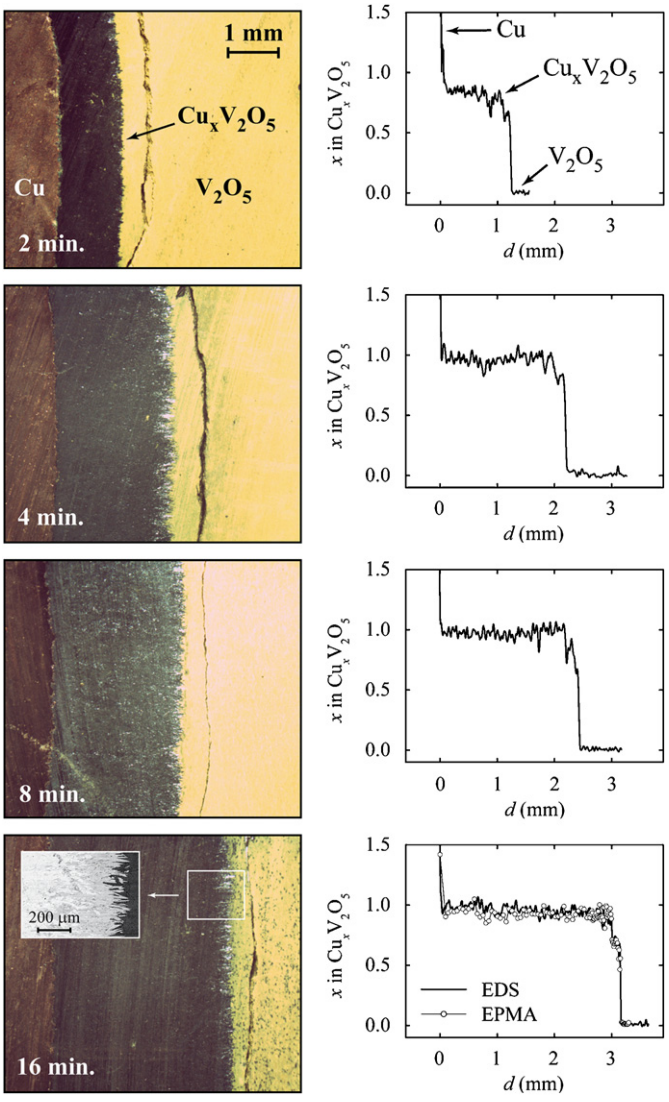

Fig. 2. Left panel: optical micrographs of samples annealed at 520 °C for 2–16 min. Metallic Cu and V_2O_5 are on either side of the micrographs, respectively. The grey-brown zone is a Cu-containing V_2O_5 phase referred to as $Cu_xV_2O_5$. The insert on the bottom micrograph (16 min) is a BSE image of the zone indicated by a white rectangle. Right panel: EDS line-scans along horizontal lines across the micrographs shown on the left panel. Cu concentration, expressed by x in $Cu_xV_2O_5$, has been determined using the calibration curve shown in Fig. 1. On the bottom figure of the right panel, an EPMA line-scan has been overlaid to the EDS line-scan. A good agreement is found between the calibrated EDS measurements and the EPMA measurements. Note the small step at d≈3 mm, which corresponds to the light grey zone of the BSE micrograph.

not constant over the whole area due to effects such as take-off angle variations. Thus, a "flattening" compensation of the EDS line-scans was performed. To evaluate the accuracy of concentrations given by EDS analyses after the signal has been corrected and calibrated following the above procedures, electron probe microanalyses (EPMA) were also performed in a Cameca SX 50 machine and compared with EDS analyses. Analytical conditions were 15 kV, 20 nA, 10 s counting time on peak and 5 s for background. Standards used were metallic Cu and V_2O_5. The agreement between EDS and EPMA is very good (see Fig. 2). Then, we evaluate the accuracy of the concentration measurements at about $\pm 10\%$. In diffusion profiles, the reference for distances d has been taken to be the interphase between metallic Cu and $Cu_xV_2O_5$ phase.

Powder X-ray diffraction patterns (PXRD) were recorded at room temperature in the 2θ range 10–60° (2θ) in steps of 0.02° and counting rates of 10 s, with a Seifert XRD 3000 diffractometer using a graphite monochromatized Cu$K\alpha$ radiation.

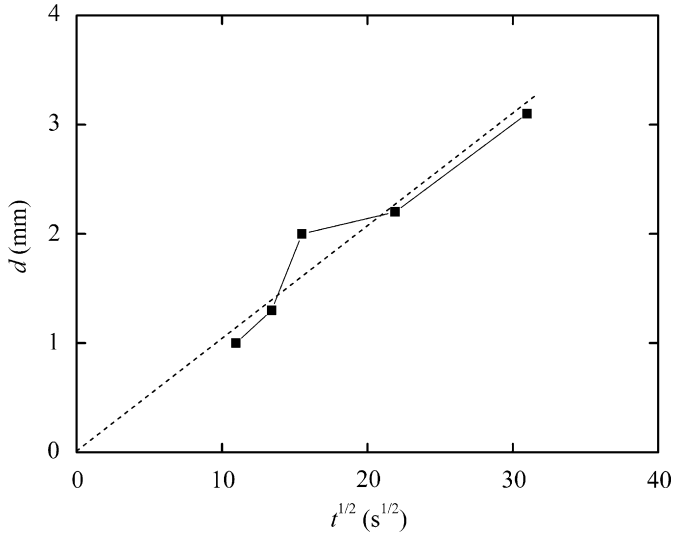

Fig. 3. Thickness (d) of the $Cu_xV_2O_5$ phase as a function of the square root of time ($t^{1/2}$). The dotted line is plotted to guide the eye. The growth rate is then parabolic in time, in line with a growth mechanism controlled by diffusion.

3. Results

Fig. 2 shows diffusion profiles of Cu into V_2O_5 at 520 °C. At first glance, the profiles exhibit a single downward step in Cu concentration. However, a closer look shows the step to be made of a second step with a plateau in the rapidly varying part of the profile (see Fig. 2, 16 min heat treatment). This plateau is not an artifact but corresponds to the light grey zone of the BSE micrograph of Fig. 2. Also the diffusion front, which looks planar, is highly irregular at a higher magnification. Then, two phases can be observed to spread from the pure Cu source, one (the more concentrated in Cu) spreading faster than the other. Fig. 3 shows measurements of the extension (d, in mm) of the mid-point of the profiles from the metallic Cu source, for different times (t, in s). The data are shown in the d vs. $t^{1/2}$ representation, since data alignment along straight lines is expected if growth mechanisms are controlled by volume diffusion.

4. Discussion

Here, the "two-step-like" shape of the diffusion profiles obtained at 520 °C (Fig. 2) is considered. This requires knowing the phase diagram of the Cu–V_2O_5 system, as well as understanding the dependence of the diffusion coefficient D on concentration, since the occurrence of phase transitions and values of D have an impact on the shape of diffusion profiles. The crystal structures of the three phases (α, β' and ε) reported in the Cu–V_2O_5 system [2] are known. The orthorhombic α phase is a doped V_2O_5 layer structure. The monoclinic β' and ε structures have been determined [8]; their projections onto the (010) plane together with their crystallographic data are given in Fig. 4. From crystallographic analysis [3], it can be reasonably assumed

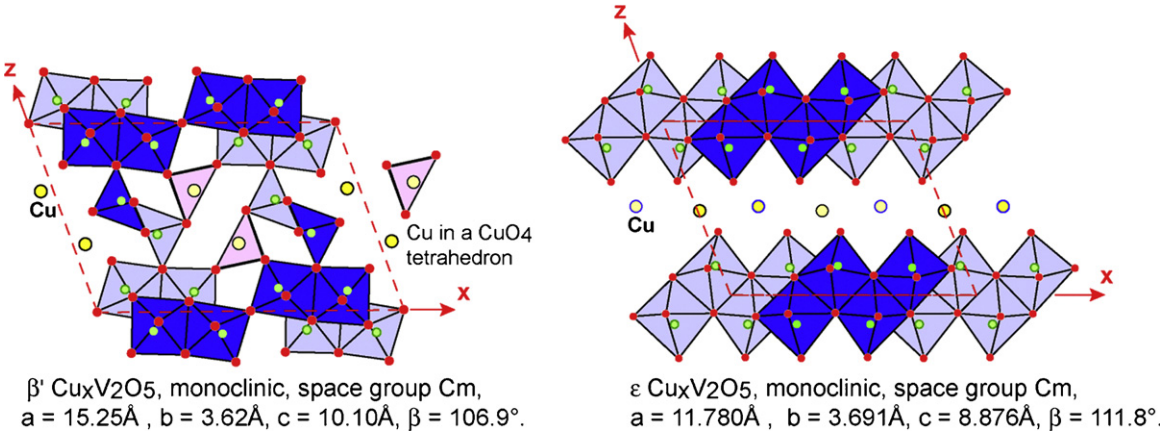

Fig. 4. Projection onto the (010) plane of the β' and the ε $Cu_xV_2O_5$ phases. Cu diffuses one dimensionally into tunnels in β' and two dimensionally between $[V_2O_5]$ layers in ε [3].

that Cu diffuses in one dimension (1D) in phase β' and in two dimensions (2D) in phase ε. Fig. 5 shows diffraction diagrams before and after diffusion of Cu in V_2O_5. The presence of phase ε is clearly seen after Cu diffusion. This

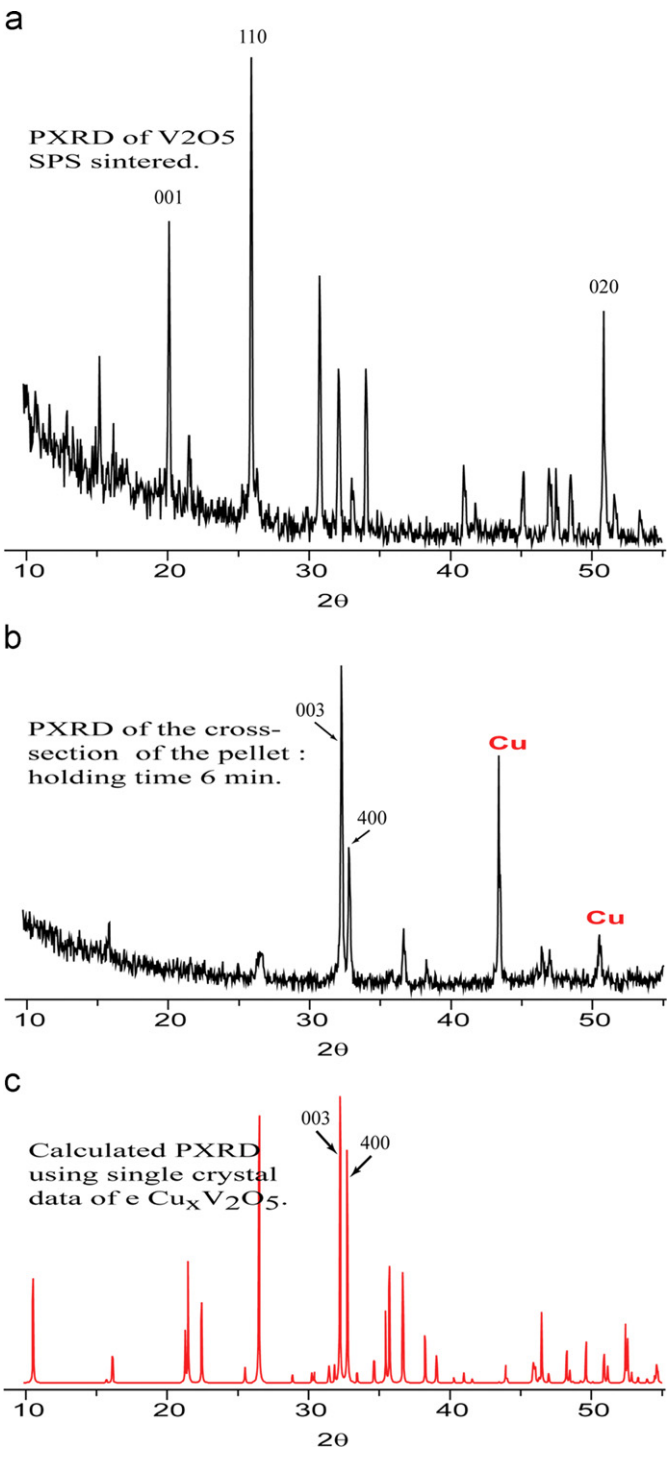

Fig. 5. PXRD of cross sections of samples compacted by SPS in identical conditions ($T = 520\,^{\circ}C$, $P = 75$ MPa): (a) pure V_2O_5, (b) Cu–V_2O_5 couple annealed for 6 min; (c) calculated PXRD of the ε-$Cu_xV_2O_5$ phase. The phase that forms when Cu diffuses in V_2O_5 is then clearly identified as ε-$Cu_xV_2O_5$. Note the strong intensity of the 0 0 3 and 4 0 0 reflections of the ε phase. This indicates a marked texture in the [h0l] direction.

phase is strongly textured along the [h0l] direction, with respect to pure V_2O_5 compacted in the same conditions.

At the temperature of our experiments (520 °C), the domains of homogeneity of phases α, β' and ε are expected to be close to those determined at 600 °C by Casalot et al. [2] (i.e. $0<x<0.02$, $0.26<x<0.64$ and $0.85<x<1$, respectively). Phases β' and ε exhibit Cu contents that can easily be measured by calibrated EDS (see Fig. 1) and EPMA line-scans. But the Cu content is too low in the α phase and its presence cannot be detected with our analytical tools. Therefore it will no longer be considered.

Diffusion profiles are affected by phase transformations and dependence of D on concentration [9], as stated above. The discussion is illustrated by calculations of diffusion profiles based on assumed dependence of D on concentration (see Fig. 6). The profiles have been generated by solving Fick's second law

$$\frac{\partial c}{\partial t} = \frac{\partial}{\partial d}\left(D\frac{\partial c}{\partial d}\right) \tag{1}$$

(with c: concentration, d: distance, t: time and D: diffusion coefficient) using a finite difference method with an implicit scheme. With this method, tridiagonal systems of equations have to be solved. This was done using a subroutine given in Ref. [10]. The phase diagram of our system is taken as an example (a schematic representation of this diagram is given in Fig. 6a). Concentration is expressed here as the value of x in $Cu_xV_2O_5$, but the discussion is also valid for similar phase diagrams in any system with concentrations expressed in atomic or weight fractions. It is assumed that the kinetics of phase growth is governed by diffusion mechanisms, as evidenced in Fig. 3.

First-order phase transformations manifest themselves as two-phase coexistence domains in the phase diagram. In the diffusion profile this leads to a vertical segment, as shown in Fig. 6b. The dependence of D on concentration is discontinuous (see Fig. 6b), because D is not defined in the concentration range of the two-phase coexistence domain. Here, D has been assumed to be equal in both phases. The next figures illustrate the influence of the dependence of D on concentration (Figs. 6c and d). Firstly, D can have different values in the different phases. Fig. 6c shows an example where D is lower in phase β' than in phase ε. It can be seen on the profile that the step corresponding to phase β' is shorter than in Fig. 6a. If the diffusion coefficient in phase β' was further reduced, the step corresponding to this phase would almost vanish and be replaced by a vertical segment. Secondly, D can vary *within* a phase. Fig. 6d gives an example of the consequence, on the diffusion profile, of a strong variation of D within phase β'. In particular, strong concentration dependence of D for a given phase can lead to an *apparent* vertical segment on the diffusion profile for the concentration range of stability of this phase. Care must be taken to avoid confusion with a *true* vertical segment coming from first-order phase transformations. Accurate knowledge of the equilibrium phase diagram is

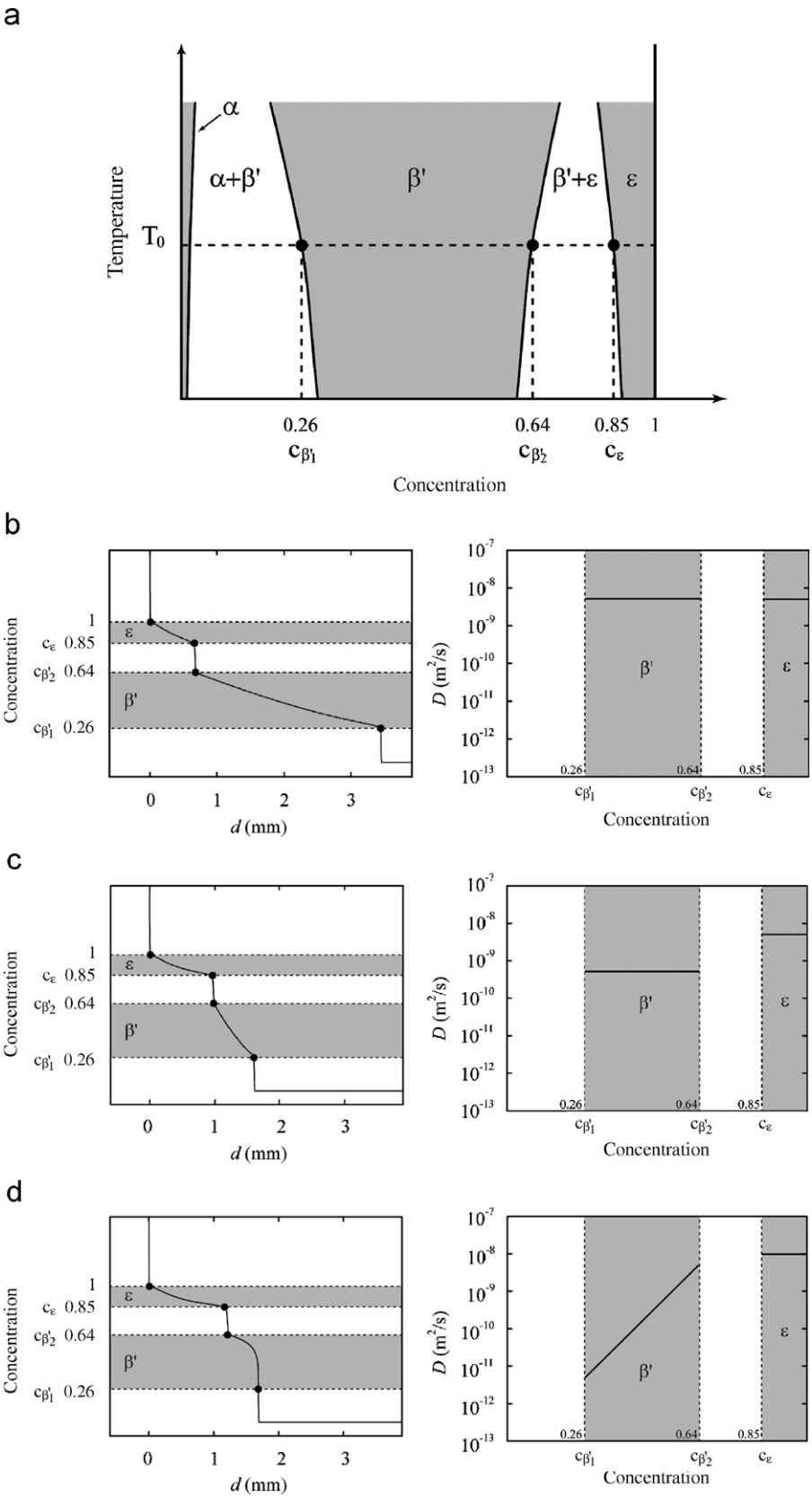

Fig. 6. (a) Phase diagram containing three phases (α, β', ε) and two two-phase coexistence domains ($\alpha+\beta'$ and $\beta'+\varepsilon$). The single-phase domains β' and ε are represented as shaded areas. Numerical values of boundaries of domains ($c_{\beta'1}$, $c_{\beta'2}$, c_{ε}) have been set to the values of the Cu–V_2O_5 system for an isothermal cut of the phase diagram at 600 °C. (b–d) Finite difference calculations of diffusion profiles assuming a dependence on concentration of diffusion coefficient D shown to the right. The single-phase domains β' and ε are shown as shaded areas (the diluted α-phase is no longer considered in the discussion). In (b), D is equal in β' and ε. In (c), D in ε is the same as in (b), while D in β' is 10 times lower than in ε. In (d), D is constant in ε, but varies over three orders of magnitude in β'. As a result the profile curvature in phase β' is inverted relative to that of the profile in phase ε. In the three cases, D is zero in the two-phase coexistence domains. Numerical values ($t = 16$ min, D as in figures) have been chosen to facilitate comparison with the profile shown in Fig. 2, 16 min.

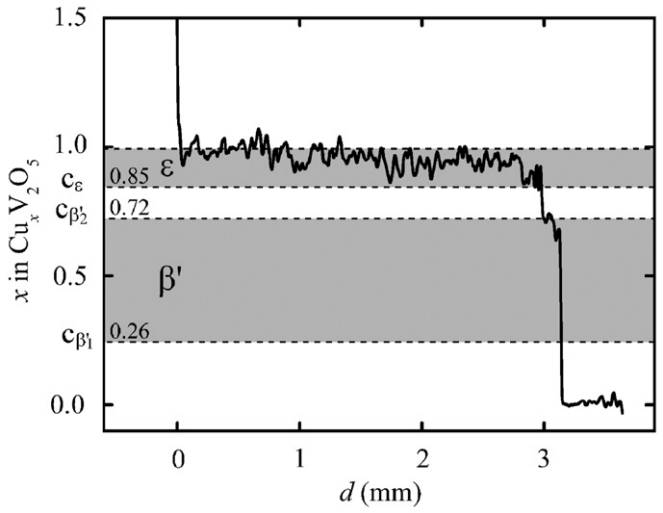

Fig. 7. Diffusion profile for $t = 16$ min. Concentration domains of phases β' and ε as given by Casalot et al. [2] are shown in grey with a slight difference relative to these authors for $c_{\beta'2}$ ($x = 0.72$ and not 0.64). However this difference is not significant. The value of $c_{\beta'1}$ is not the result of a visible accident in the curve and we have reported the value given by Casalot et al. ($c_{\beta'1} = 0.26$ [2]). The boundaries of phase ε are in good agreement with those of these authors ($x = 0.85$ and 1).

then necessary to properly interpret shapes of diffusion profiles.

Fig. 7 shows a diffusion profile after 16 min at 520 °C with an overlay of the stability ranges for phases β' and ε. This profile is of the type given in Fig. 6d. The diffusion coefficient in phase ε is roughly independent of concentration. Its value has then been calculated using Crank's "one-step" diffusion coefficient analysis [9], in which the diffusion coefficient D is assumed to be uniform inside the concentration interval $[c, c_0]$ and equal to zero outside. To obtain the value of D, the following equation has to be solved:

$$\frac{c - c_0}{\sqrt{\pi} K \exp(K^2)\mathrm{erf}(K)} + c = 0, \quad (2)$$

with

$$K = \frac{d/\sqrt{t}}{2\sqrt{D}}, \quad (3)$$

with c_0: concentration at the interface with the source of diffusing species, c: concentration at the edge of the step, d: distance of extension of the step from the source and t: time. The erf function has been approximated by a polynomial. In our case, $c_0 = 1$, $c = 0.85$ (see Fig. 7), then Eq. (2) gives $K = 0.29$. In Eq. (3) the numerator is the slope of the regression line of the data given in Fig. 3. From this, we find $D \approx 3 \times 10^{-8}$ m^2/s. This is a remarkably high value, of the same order of magnitude as the self-diffusion coefficients of liquid metals. It is also indicative of a high mobility for the Cu atoms between the $[V_2O_5]$ layers in the concentrated phase ε. In contrast, to account for the shape of the diffusion profile in phase β', the diffusion coefficient has to vary significantly (over several orders of magnitudes) in the composition range of this phase (see Fig. 6d). Indeed, an inversion of the profile curvature in phase β' with respect to that in phase ε can only occur if D varies as in Fig. 6d. This significant dependence on concentration of the diffusion coefficient within phase β' leads to the formation of an *apparent* vertical segment on the diffusion profile. Finally, D in phase β' is much lower than in phase ε, but it is difficult to give a more accurate value, given the perturbed shape of the growth front of phase β' (see Fig. 2, 16 min).

The observed strong dependence of D on concentration in phase β' may seem surprising, since no major structural change occurs in this phase when Cu concentration varies. However, strong influence of concentration on D has been predicted by Monte Carlo simulations [11] for volume diffusion and by molecular dynamics simulations for surface diffusion [12]. In both cases, D can vary over several orders of magnitude when the concentration of the diffusing species changes. In Murch and Thorn's work [11], 2D diffusion of Na^+ ions into a honeycomb lattice of β'' alumina was simulated. In our case, however, Cu ions diffuse in 1D in phase β' [3]. But it seems that the major trends reported in Murch and Thorn's calculations can be found in our experiments. In these simulations, the dependence on concentration of D was due to strength and direction (attractive or repulsive) of the interactions between the diffusing ions. D increased with concentration for repulsive interaction and the reverse occurred for attractive interactions. In our case, the increase in diffusion coefficient with Cu concentration is in good agreement with the fact that Coulombic forces between Cu ions are repulsive.

Both regimes, i.e. fast extension of phase ε and comparatively slower extension of phase β', can be interpreted by using the differences in diffusion mechanisms (2D and 1D diffusion). In 2D, Cu atoms are expected to have greater freedom and therefore a higher mobility than in 1D. In addition, Cu concentration differences in these phases lead to strong differences in the collective diffusion mechanisms (as simulated by Murch and Thorn [11]). In particular, the increase in diffusion coefficient with an increase in concentration should occur even in the case of phase transformation. Then, it is not surprising that the growth rate of the concentrated ε phase is higher than that of the comparatively less concentrated β' phase.

The strong texturation that accompanies the synthesis of ε phase from the original V_2O_5 phase (Fig. 2) may also impact the kinetics of Cu atoms diffusion. This phenomenon is indeed spectacular since it involves recrystallization of the complex V_2O_5 structure within very short times. The irregular shape of the diffusion front (see Fig. 2) with elongated crystallites oriented in the same direction is a result of this process. The mechanisms by which the V_2O_5 crystal structure transforms to ε phase when Cu atoms are inserted have been analysed previously [3]. Cu insertion between every two successive $[V_2O_5]_n$ single layers slightly closes the interlayer and generates rotation of VO_5 square

pyramids. Then, the single layers slip parallel to each other and collapse to form the double-layered structure typical of the ε phase. We suppose that the mechanisms by which the texturation along the [h0l] direction occurs are closely related to this crystallographic reorganization, but a more accurate explanation is still lacking, as well as the impact of this texturation on the diffusion kinetics of Cu.

Also worth discussing is the effect of the current applied to the samples during compaction by SPS on the diffusion mechanisms. Or to put it differently, is there an electromigration mechanism involved in our experiments in addition to the classical Fickian diffusion. Indeed it is well known (e.g. [5]) that current densities of the order of magnitude of those applied during an SPS process ($\approx$100–1000 A/cm^2) often greatly impact diffusion processes. This kind of effect could potentially affect the measurement of diffusion coefficients. However, only in conducting materials can high current densities be present. As V_2O_5 is not a good conductor, current lines avoid the sample and only flow through the carbon die. Thus it can be assumed that the sample is almost free of current, and no significant electromigration effects can modify our results.

5. Conclusion

Rapid SPS compaction has allowed us to study fast diffusion phenomena occurring in the Cu–V_2O_5 system. Two phases exhibit significant growth at 520 °C. In the more Cu-concentrated one, i.e. phase ε, the diffusion coefficient is roughly equal to 3×10^{-8} m^2/s, that is, of the order of magnitude of self-diffusion in liquid metals. This is a remarkably high value. In the less Cu-concentrated phase, i.e. phase β', the diffusion coefficient is lower. These two regimes are assumed to result from differences in diffusion mechanisms in phases ε and β', i.e. 2D and 1D diffusion, respectively. In addition, while the diffusion coefficient does not significantly change with composition variations in phase ε, its value varies over several orders of magnitude with composition in phase β'. This marked dependence on concentration has been theoretically predicted as resulting from repulsive interactions between the diffusing atoms.

Acknowledgments

This work has been performed with the Syntex 2080 SPS machine of the "Plateforme Nationale de Frittage Flash du CNRS", set up by Patrice Millet and Jean Galy (2003–2004), located in the Module de Haute Technologie de l'Université Paul Sabatier Toulouse III. We are grateful to Mr. Jacques Crestou of CEMES-CNRS for his help with sample preparation. We thank Mr. Lucien Datas and Mr. Stéphane Le Blond du Pouy of the "Service Commun de Microscopie" for performing the SEM and EDS experiments and Mr. Philippe de Parseval of the "Laboratoire des Mécanismes et Transferts en Géologie—CNRS" for performing the EPMA analyses, on the Université Paul Sabatier Toulouse III campus.

References

[1] M. Morcrette, P. Rozier, L. Dupont, E. Mugnier, L. Sannier, J. Galy, J.-M. Tarascon, Nat. Mater. 2 (2003) 755–761.
[2] A. Casalot, A. Deschanvres, P. Hagenmuller, B. Raveau, Bull. Soc. Chim. Fr. XC (1965) 1730–1731.
[3] J. Galy, J. Solid State Chem. 100 (1992) 229–245.
[4] A.V. Chadwick, Defect Diffus. Forum 83 (1992) 235–258.
[5] Z.A. Munir, U. Anselmi-Tamburini, M. Ohyanagi, J. Mater. Sci. 41 (2006) 763–777.
[6] H. Conrad, Mater. Trans. 46 (2005) 1083–1087.
[7] M. Eriksson, Z. Shen, M. Nygren, Powder Metall. 48 (2005) 231–236.
[8] J. Galy, D. Lavaud, A. Casalot, P. Hagenmuller, J. Solid State Chem. 2 (1970) 531–543.
[9] J. Crank, The Mathematics of Diffusion, Clarendon Press, Oxford, 1956.
[10] W.H. Press, B.P. Flannery, S.A. Teukolsky, W.T. Vetterling, Numerical Recipes in FORTRAN 77: The Art of Scientific Computing, Cambridge University Press, Cambridge, 1992.
[11] G.E. Murch, R.J. Thorn, Philos. Mag. 35 (1977) 493.
[12] J. Moon, P. Yoon, P. Wynblatt, S. Garoff, R.M. Suter, Comput. Mater. Sci. 25 (2002) 503.